ADVANCES IN ATMOSPHERIC SCIENCES, VOL. 38, SEPTEMBER 2021, 1474–1485

• **Original Paper** •

Thinner Sea Ice Contribution to the Remarkable Polynya Formation North of Greenland in August 2018

Xiaoyi SHEN[1,2,3], Chang-Qing KE[*1,4], Bin CHENG[5], Wentao XIA[1,2,3], Mengmeng LI[1,2,3], Xuening YU[1,2,3], and Haili LI[1,2,3]

[1]*School of Geography and Ocean Science*, *Nanjing University*, *Nanjing* 210023, *China*

[2]*Jiangsu Provincial Key Laboratory of Geographic Information Science and Technology*, *Nanjing University*, *Nanjing* 210023, *China*

[3]*Collaborative Innovation Center of South China Sea Studies*, *Nanjing University*, *Nanjing* 210023, *China*

[4]*Collaborative Innovation Center of Novel Software Technology and Industrialization*, *Nanjing* 210023, *China*

[5]*Finnish Meteorological Institute*, *Helsinki* 00101, *Finland*

(Received 6 May 2020; revised 21 January 2021; accepted 22 March 2021)

ABSTRACT

In August 2018, a remarkable polynya was observed off the north coast of Greenland, a perennial ice zone where thick sea ice cover persists. In order to investigate the formation process of this polynya, satellite observations, a coupled ice-ocean model, ocean profiling data, and atmosphere reanalysis data were applied. We found that the thinnest sea ice cover in August since 1978 (mean value of 1.1 m, compared to the average value of 2.8 m during 1978–2017) and the modest southerly wind caused by a positive North Atlantic Oscillation (mean value of 0.82, compared to the climatological value of –0.02) were responsible for the formation and maintenance of this polynya. The opening mechanism of this polynya differs from the one formed in February 2018 in the same area caused by persistent anomalously high wind. Sea ice drift patterns have become more responsive to the atmospheric forcing due to thinning of sea ice cover in this region.

Key words: polynya, sea ice thickness, wind, sea ice drift, Greenland

Citation: Shen, X. Y., C.-Q. Ke, B. Cheng, W. T. Xia, M. M. Li, X. N. Yu, and H. L. Li, 2021: Thinner sea ice contributes to the remarkable polynya formation in August 2018, north of Greenland. *Adv. Atmos. Sci.*, **38**(9), 1474–1485, https://doi.org/10.1007/s00376-021-0136-9.

Article Highlights:

- A polynya was observed in August 2018 north of Greenland in a perennial ice zone.
- Thinner sea ice cover played a critical role on the formation of this polynya.
- Sea ice drift has become more responsive to the regional wind favoring polynya formation because sea ice has become thinner.

1. Introduction

The term "polynya" refers to a large opening among the sea ice pack that remains ice-free or is only covered by thin ice for a time period (a minimum timespan of ~15 days). Generally, there are two types of polynya, i.e., latent heat polynya and sensible heat polynya. The former forms from persistent wind which drives the sea ice away from a barrier (e.g., coast, fast ice and ice shelf); the latter is driven by thermodynamic factors, e.g., the warm water upwelling which melts the sea ice cover. In the Arctic, polynyas usually appear around the Arctic shelf areas (e.g., Siberian Shelf and Beaufort Shelf regions, Preußer et al., 2016), increase the heat extraction from the ocean to the atmosphere [e.g., an increase of approximate 150 W m^{-2} in the heat extraction from the ocean is due to polynyas forming; Martin et al. (2004)] and affect the sea ice production [e.g. 70 km^3 per year; Martin et al. (2004)]. Thus, they can serve as a new proxy for weather and climate variations (April et al., 2019).

Sea ice north of Greenland is among the oldest multi-year ice (MYI) zones in the Arctic. In the past 30 years, a decline of more than 50% in MYI area has been observed in the Arctic (Kwok, 2018). In February 2018, extremely high

* Corresponding author: Chang-Qing KE
Email: kecq@nju.edu.cn

wind (higher than 25 m s^{-1}) led to the development of a polynya in the Wandel Sea. Such a pronounced polynya has never been observed before in this region at that time of year since 1979 (Moore et al., 2018; Ludwig et al., 2019). In August 2018, a polynya was observed again. It appeared north of Kap Morris Jesup, developed rapidly towards the Lincoln Sea (west of 40°W) and eventually extended along the north coast of Greenland (covering the area between 15°–45°W).

The formation of polynyas in the Arctic is mostly determined by regional wind (Smith et al., 1990), and it has been found that high wind played an essential role in the February polynya formation (Moore et al., 2018). In summer, thermodynamic effects, e.g., ocean-to-atmosphere heat fluxes (Minnett and Key, 2007), ocean interior salt fluxes (Martin et al., 2004) and transport of upwelling oceanic heat (Campbell et al., 2019), are also critical. However, a full explanation for the August polynya formation is still not established. Understanding the mechanism, including both dynamic and thermodynamic processes for sudden opening of summer polynyas is still a challenging task.

In this study, we applied a set of comprehensive data to investigate 2018 August polynya formation, i.e., to analyze the effects of atmosphere, sea ice and ocean on the polynya occurrence. Satellite and in situ observations were used to identify the evolution of this polynya. In situ observations of sea ice thickness (SIT) and ocean interior properties (e.g., ocean temperature, salinity and density) are very limited to the north of Greenland (e.g., ice mass balance buoy data, http://imb-crrel-dartmouth.org/archived-data). Hence, SIT model data from the Pan-Arctic Ice-Ocean Modelling and Assimilation System (PIOMAS) were used to investigate the ice thickness. Ocean interior temperature and salinity during the polynya period were detected using weekly gridded ocean temperature and salinity profiling data (generated from European Union (E.U.) Copernicus Marine Service Information). European Centre for Medium-Range Weather Forecasts (ECMWF) ERA5 reanalysis data as well as a large-scale atmospheric circulation index (i.e., North Atlantic Oscillation, NAO) were also applied here.

2. Data and methods

Sea ice concentration (SIC) data were obtained from the National Snow and Ice Data Center (NSIDC) Nimbus-7 Scanning Multichannel Microwave Radiometer (SMMR) and Defense Meteorological Satellite Program (DMSP) Special Sensor Microwave Imager (SSM/I)–Special Sensor Microwave Imager/Sounder (SSMIS) passive microwave observations (Parkinson et al., 1996; Cavalieri et al., 1997), which were produced using a revised National Aeronautics and Space Administration (NASA) Team algorithm. Daily products at a grid cell size of 25 × 25 km for the period 1979–2018 were used. SIT data were taken from the PIOMAS model (Zhang and Rothrock, 2003), and a monthly product with a spatial resolution of 1° (latitudinal direction) × 2.67° (longitudinal direction) for the period 1978–2018 was used. NSIDC sea ice drift data (Tschudi et al., 2019) were used to calculate sea ice drift speed. Daily products with a spatial resolution of 25 × 25 km for the period 1979–2018 were used.

Weekly gridded ocean temperature and salinity profiling data were obtained from the E.U. Copernicus Marine Service Information MULTIOBS_GLO_PHY_NRT_015_001 dataset. The weekly product with a spatial resolution of 0.25° × 0.25° was obtained for the period 2014–18. This dataset is a combination of satellite and in situ data [for details see Guinehut et al. (2012) and Mulet et al. (2012)].

Hourly 2-m air temperature (T2m), 10-m level wind speed/direction and surface sensible heat flux data with a spatial resolution of 0.25° × 0.25° were taken from the ECMWF ERA5 reanalysis data. Daily mean values were calculated for analysis. The daily NAO index was obtained from the Climate Prediction Center of National Oceanic and Atmospheric Administration (NOAA) for the period 1972–2018.

Meteorological data from the weather station at Kap Morris Jesup (83.65°N, 33.37°W) were used to analyze the local weather conditions. We used observations of T2m and wind speed/direction. The time step of observed data was 6 hours, and each observation was averaged daily in the present study.

Moderate Resolution Imaging Spectroradiometer (MODIS) true-color combination imagery from NASA Worldview application, part of the NASA Earth Observing System Data and Information System (EOSDIS) were used. These images are the combination of MODIS level-1B reflectance images with a spatial resolution of 250 m, using band 1 (approximately 0.62–0.67 μm wavelength), band 4 (approximately 0.54–0.57 μm wavelength) and band 3 (approximately 0.46–0.48 μm wavelength) as the red, green and blue channels, respectively.

The region of interest (ROI) was defined as 55°W–5°E and 82°–85°N, in which the polynya occurred. Unless otherwise stated, average values calculated within the ROI for all gridded fields were used to analyze the ice, ocean and atmosphere conditions. We calculated the time-series on the original grid cells of the respective dataset and used a SIC threshold of 50% for a definition of the polynya region, i.e., grid cells with SIC less than 50% were defined as polynya grid cells. The polynya extent was comprised of all grid cells below 50% SIC within the ROI. The polynya extent was defined as the surface area of all SIC grid cells below 50% (i.e., not weighted by SIC). The average SIC and polynya extent were calculated for each day.

3. Results and discussions

3.1. *Formation of polynya and local meteorological conditions*

On 29 July 2018, in the middle of the melting period, no polynyas or leads were observed (Fig. 1a). The average

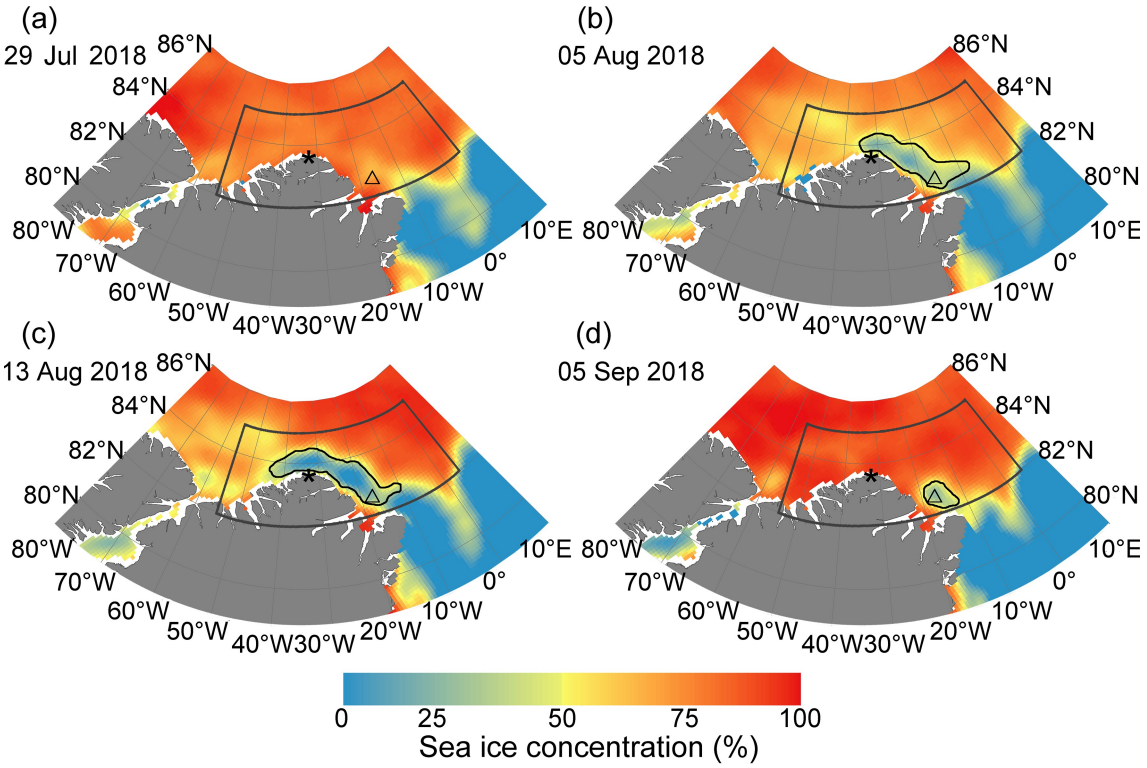

Fig. 1. Sea ice concentration evolution between late July and early September, north of Greenland in the Arctic Ocean. Black polygons indicate the region of interest where the polynya was observed. Black curves indicate the boundaries of the polynya. The location of the Kap Morris Jesup weather station is marked as *. The location of the Wandel Sea is marked as △. Sea ice concentration data are taken from NSIDC.

SIC in the ROI was almost 98% (Fig. 2a) and the T2m was about 0.28°C (Fig. 2b). On 5 August, a polynya developed in the Wandel Sea (Fig. 1b, the location is marked as triangle) with an extent of approximately 4.4 × 10^3 km^2 (Fig. 2a), accompanied by the continued above-freezing T2m since the beginning of August (Fig. 2b). On 13 August, this polynya was observed to cover areas west of 40°W (Fig. 1c) with an extent of 11.3 × 10^3 km^2 and a T2m of 0.69°C (Fig. 2b and 2c). The extent of this polynya subsequently expanded until it reached its maximum size on 18 August (about 17.5 × 10^3 km^2, Fig. 2a). On 5 September, the SIC in the ROI had returned to climatological values (Fig. 2a) with a T2m of −5.97°C (Fig. 2b).

The daily-mean T2m and wind speed observed at Kap Morris Jesup weather station during the polynya period are shown in Fig. 3. From 15 July to 31 August, the average T2m was 4.9°C with standard deviation of 4.4°C, and the maximum T2m was 12°C. From 1 September onward, the T2m dropped below freezing. The average wind speed was 3.6 m s^{-1} while the standard deviation was 1.9 m s^{-1}, and the average wind direction observed at the Kap Morris Jesup weather station was 28° west of due south (offshore). The warm and moderate southerly wind are consistent with the formation of August polynya.

3.2. *Environment factors linked to polynya development*

To investigate the environmental factors linked to the polynya formation and development, we present a comprehensive analysis of the atmosphere, sea ice and ocean conditions during the polynya period. Although the polynya appeared suddenly on 3 August, to investigate the effect of various environment factors, we carried out the data analyses from the beginning of 2018.

3.2.1. *The role of the atmosphere*

Usually, the contribution of the atmosphere to the polynya formation can be attributed to two aspects. First, sea ice melts due to high air temperatures; second, sea ice drift occurs under regional wind (a combination of wind speed and direction drives the sea ice drift). Although the T2ms were high in summer, they barely reached the freezing point (Fig. 2b) and thus can only lessen the sea ice refreezing. Hence, air temperature is not enough to explain the polynya formation and development. It is expected that wind is dominant for the polynya initial formation and further development, while the high temperatures lessened refreezing and thus aided in maintaining the polynya development.

3.2.1.1. Sea ice drift driven by wind

Winds can alter sea ice cover by causing sea ice drift, especially when the sea ice cover is quite thin. Here we examined the relationship between the polynya extent evolution and the cumulative wind-speed anomaly from the aver-

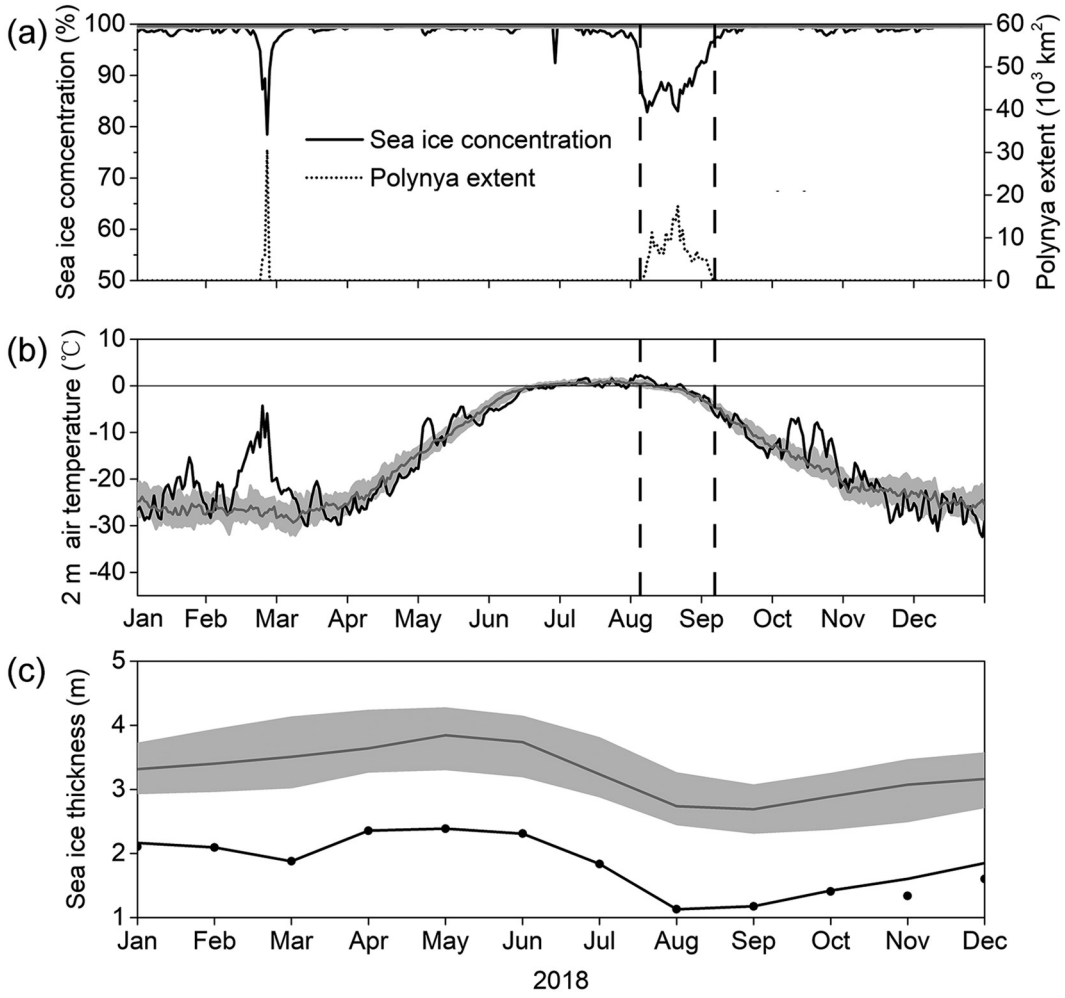

Fig. 2. (a) Daily sea ice concentration; (b) daily 2-m air temperature and (c) monthly sea ice thickness in the region of interest. Daily values through 2018 of sea ice concentration and 2-m air temperature, and monthly values of sea ice thickness are shown as solid black lines. The climatological values (1979–2018) are shown as the medians (grey lines), and the 25%–75% interquartile range is marked by grey shading. The polynya extent is shown as a dotted line in (a). It should be noted that the climatological values for SIC are also provided in (a), and that their values are quite close to 100%. The black horizontal line in (b) is the freezing point. The vertical black dashed lines in (a) and (b) indicate the polynya period. The black line in (c) shows the monthly sea ice thickness in 2018 in the region of interest, and the black dot denotes the monthly minimum sea ice thickness during 1979–2018. The sea ice concentration, air temperature and sea ice thickness are taken from NSIDC, ERA5 data and PIOMAS model, respectively.

age value during the August polynya period (Fig. 4a). The cumulative wind-speed anomaly, which was calculated from the sum of the wind speed anomaly from the average value during the time period between 15 July and 13 September, can reveal the degree of the wind speed anomaly in a time period. A high correlation coefficient (0.68, p-value < 0.01) indicates that the polynya expansion was associated with the local wind. On 3 August when the polynya started to open, a positive ocean–atmosphere sensible heat flux of 52 W m^{-2} (Fig. 4c, vertical fluxes are positive downwards) associated with warm southerly wind (observed at the Kap Morris Jesup weather station) caused the heat exchange from the atmosphere to ocean. This heat exchange may have created more heat into the ocean, which would contribute to the maintenance of the polynya and further affect the water mass transformation and deep water formation (Moore and Pickart, 2012).

Although local wind was found to be associated with the polynya opening, the wind speeds in the ROI during polynya period were moderate. According to the ERA5 data, the wind speeds during August 2018 (3.8 m s^{-1}, Fig. 5b) were mostly within the climatological ranges and at a relative minimum compared to other times of the year. Figure 5c shows the wind directions in August 2018 accompanied with the average wind direction during August 1979–2017. The average wind direction pattern is normally northward flow during August 1979–2017, and this is similar to that in August 2018. Both wind speeds and directions (Figs. 5b and 5c) were comparable to these in previous years, hence regional wind is not the determining factor to cause the

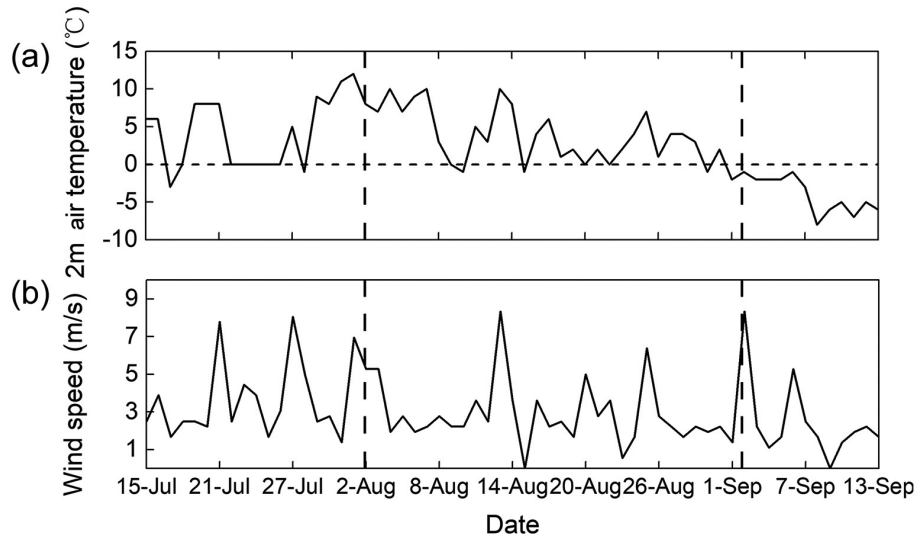

Fig. 3. (a) 2-m air temperature and (b) wind speed from 15 July to 13 September 2018 observed at Kap Morris Jesup weather station. Black horizontal dashed line in (a) is the zero-degree temperature. Black vertical dashed lines indicate the polynya period. These data are sub-daily measurements and averaged daily here.

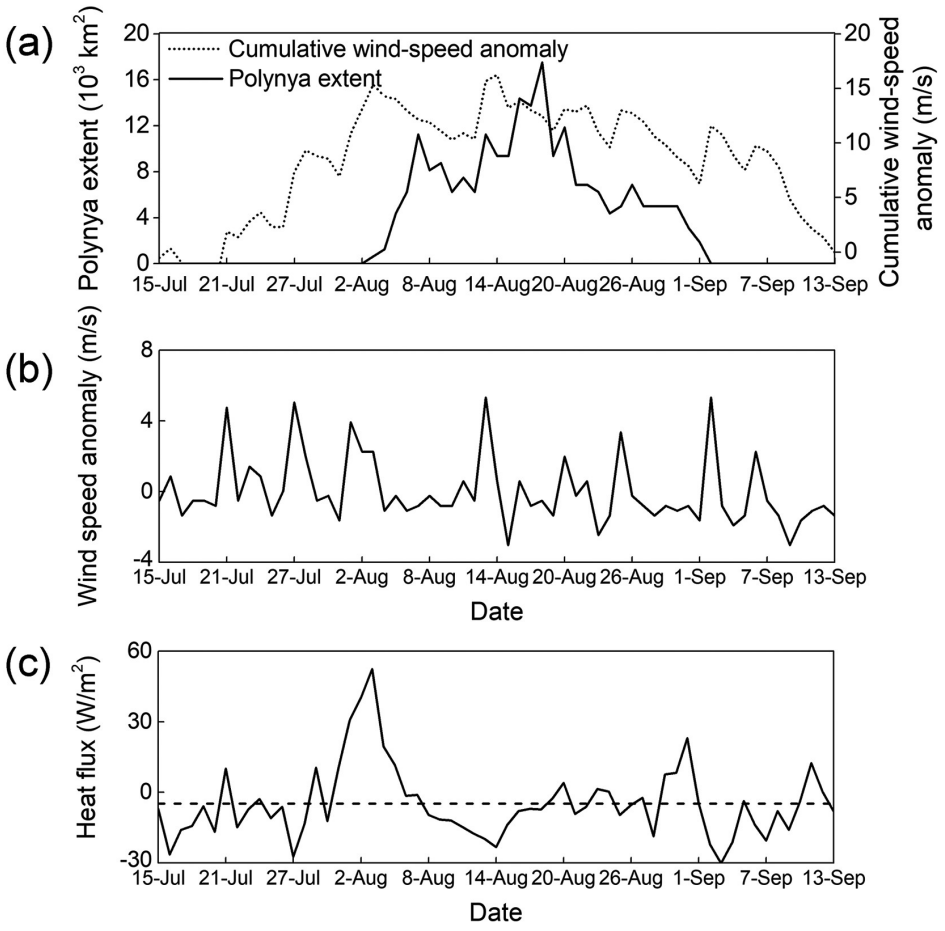

Fig. 4. Polynya extent, weather parameters and surface heat flux between 15 July and 13 September 2018. (a) Daily polynya extent (solid line) and cumulative wind-speed anomaly (dot line) based on (b); (b) wind speed anomaly from the average value at Kap Morris Jesup weather station and (c) The spatial average sensible heat flux (solid) and an average sensible heat flux during the polynya period (dashed) estimated from ERA5 data in the region of interest. The flux is positive downward.

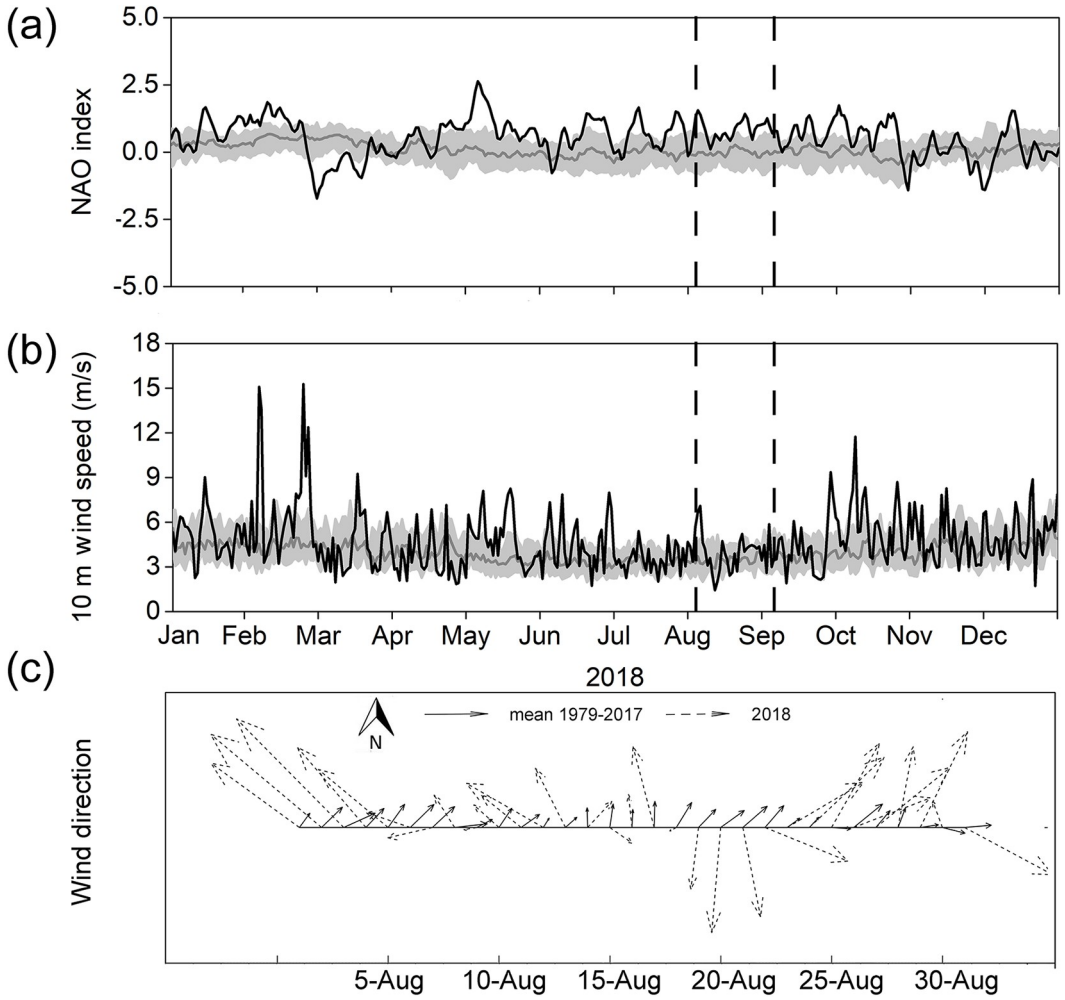

Fig. 5. The atmospheric circulation index and wind speed/direction in the region of interest. (a) North Arctic Oscillation index; (b) 10 m wind speed; (c) wind direction in August 2018. For (a) and (b), daily values are shown by black lines, associated climatological values (1979–2018) are shown by the medians (grey lines) and the 25%–75% interquartile range are marked by grey shading. Black dashed lines in (a) and (b) indicate the polynya period. NAO index values are taken from NOAA, 10 m wind speed and direction are taken from ERA5 data. The arrows in (c) only represents the direction, their length cannot be used to indicate the wind speed.

polynya opening. Instead, some other factors appear to have made sea ice drift stronger than expected, under the modest wind speeds.

The average August SIT in 2018 in the ROI was the minimum since 1979 (Fig. 2c), according to the PIOMAS model. The continued decrease in SIT during the past 40 years contributed to the minimum in 2018. The SIT anomaly may be responsible for the polynya opening as thinner sea ice tends to be easier to drift (Kwok et al., 2013). In order to test this assumption off the north coast of Greenland, we examined the relationship between wind speeds and ice drift speeds in different periods with different SIT conditions (Table 1). Correlations between wind speeds and ice drift speeds tend to be higher when ROI SIT decreases, which indicates that the sea ice drift has become more responsive to atmospheric forcing due to sea ice thinning in this area. In addition, it was also found that most of the MYI was replaced by first-year ice (FYI) due to the February polynya along the north coast of Greenland (Ludwig et al., 2019), and this persisted throughout the winter. Hence, the unusual conditions during the winter of 2018 also played an important role in the August polynya formation, as thin FYI is easier to drift than thick MYI.

3.2.1.2. Spatial pattern of sea ice drift

Sea ice drift can be caused by both wind and oceanic current. Due to the lack of the observations of oceanic current, it is impossible to estimate the quantitative contributions of oceanic current to the sea ice drift. Kwok et al. (2013) used a squared correlation coefficient to describe the fraction of the variance of sea ice drift which can be explained by the geostrophic wind. They found a correlation coefficient of 0.80 in summer from 1982–2009, i.e., wind can explain all but about 36% of the variance of sea ice drift. As the sea ice

Table 1. Sea ice thickness, wind speed and sea ice drift speed in the region of interest in different periods from August 1979–2018. Correlations between wind speeds and sea ice drift speeds are also shown in table, correlation coefficients that were significant at the 95% confidence level according to two-tailed Student's *t*-tests are shown in bold.

	1979–1988	1989–1998	1999–2008	2009–2018	1979–2017	2018
Sea ice thickness (m)	3.2 ± 0.4	3.1 ± 0.5	2.7 ± 0.4	2.3 ± 0.4	2.8 ± 0.5	1.1 ± 0.5
Wind speed (m s^{-1})	4.4 ± 0.3	4.7 ± 0.5	4.4 ± 0.5	4.4 ± 0.8	4.5 ± 0.5	4.0 ± 1.3
Sea ice drift speed (cm s^{-1})	3.8 ± 0.3	5.4 ± 1.7	4.1 ± 1.3	6.0 ± 2.2	4.9 ± 1.7	3.9 ± 2.0
Correlation	−0.10	**0.85**	**0.88**	**0.90**	**0.73**	–

cover is trending towards being thinner and weaker, this coefficient near the ice edge is expected to be higher in the future (Kwok et al., 2013). Hence, wind is an essential factor to affect the sea ice drift compared to the ocean currents.

The spatial pattern of wind is usually inhomogeneous; thus, the sea ice drift is also not uniform. Regionally-averaged ice drift vectors may hide the details of the spatial pattern of sea ice drift. While the sea ice divergence (calculated from sea ice drift vectors) can reveal detailed sea ice drift patterns, the sea ice drift product is more uncertain in areas of low SIC (Sumata et al., 2014). In the present study, time-series of MODIS images in August 2018 shown in Fig. 6 reveal the spatial pattern of sea ice drift, accompanied by the local wind vectors (red arrows, taken from ERA5 data). The sea ice drift vectors (blue arrows) were determined based on visual interpretation of MODIS image sequences. In general, quite consistent spatial patterns between the wind and sea ice drift fields can be seen in Fig. 6. This also confirmed that wind played a more essential role in sea ice motion (Kwok et al., 2013). On 11, 14, 19, 21 and 28 August when northerly winds occurred, the polynya coverage shrank. On other days with a southerly wind, the polynya expanded. Thus, the changes in prevailing direction of the wind (and associated sea ice drift) were consistent with the polynya evolution. This indicates that wind is the direct factor for August polynya formation. However, as was mentioned before, neither the wind speed nor direction in August 2018 were anomalous, thus the sea ice drift became more responsive to the regional wind favoring polynya formation when sea ice was getting thinner. Hence, thinner sea ice cover played a relatively greater role in the polynya formation.

3.2.1.3. The role of the large-scale atmosphere circulation

Large-scale atmosphere records were also examined (hereafter, wind speed data were derived from the ERA5 reanalysis data, Fig. 5). During the polynya period, the climate records showed positive NAO phases (mean value of 0.82, compared to climatological value of −0.02), which were accompanied by a modest wind speed (3.8 m s^{-1}, comparing to climatological value of 4.2 m s^{-1} and averaged value of 4.5 ± 0.6 m s^{-1} during 1979–2017), with correlation coefficients of 0.51 (p-value < 0.01) in the ROI. In addition, a positive phase of the NAO index in August is associated with a low pressure anomaly over Greenland and therefore southeasterly wind anomalies in the ROI (Fig. 5c). Although NAO showed positive phases during polynya periods, its associated wind speeds were not anomalous in comparison to the climatological values (Fig. 5). Thinner sea ice cover increased the responsiveness of sea ice drift to wind, which indicates that polynyas are more susceptible to forming in this region under normal atmospheric conditions (i.e., the MYI area north of Greenland has become less resilient with respect to latent heat polynya formation).

3.2.2. *The role of the ocean*

The temperature and salinity mainly control ocean stratification under sea ice (e.g., Campbell et al., 2019); hence, they can be used to reveal ocean interior property changes (e.g., heat/salinity upwelling). The upwelling induced by wind stress and subsequent Ekman divergence/offshore transport in the upper layer may bring the sub-surface heat to the surface, which can contribute to maintaining the polynya. Ocean profiling data shows that mixed-layer temperatures during the August polynya period were about 0.1°C higher than climatological values (Fig. 7a), whereas the mixed-layer salinity and depth were within the climatological range (Figs. 7b and 7c).

Following the polynya opening, temperature dropped only to −1.7°C from −1.5°C and salinity remained at 33 psu at a depth of 50 m in the ocean interior based on ocean property profiling data (Fig. 8). Thus, there is no evidence for the occurrence of upward heat flux in the polynya period. Upwelling of intermediate Atlantic water would result in ocean warming and salinification. Oceanic heat played a weaker role in August polynya formation than wind forcing, and therefore this polynya is classified as a latent heat polynya.

On the other hand, sea ice may be subject to wind-induced wave impact and break off, especially under the influence of storm-generated waves (Kohout et al., 2014). Although the significant wave height (SWH) values near the sea ice edge suggest there was potential to break up the sea ice cover north of Greenland due to the thinner thickness, no major storms were observed prior this polynya event, and the wind speed pattern was not unusual. We may conclude that the impact of ocean waves on polynya formation in this case was minor. The effect of waves on ice break-up largely depends on the SWH at the ice edge and the distance between the ice cover and ice edge (Squire and Moore, 1980). A better quantitative estimation of wave

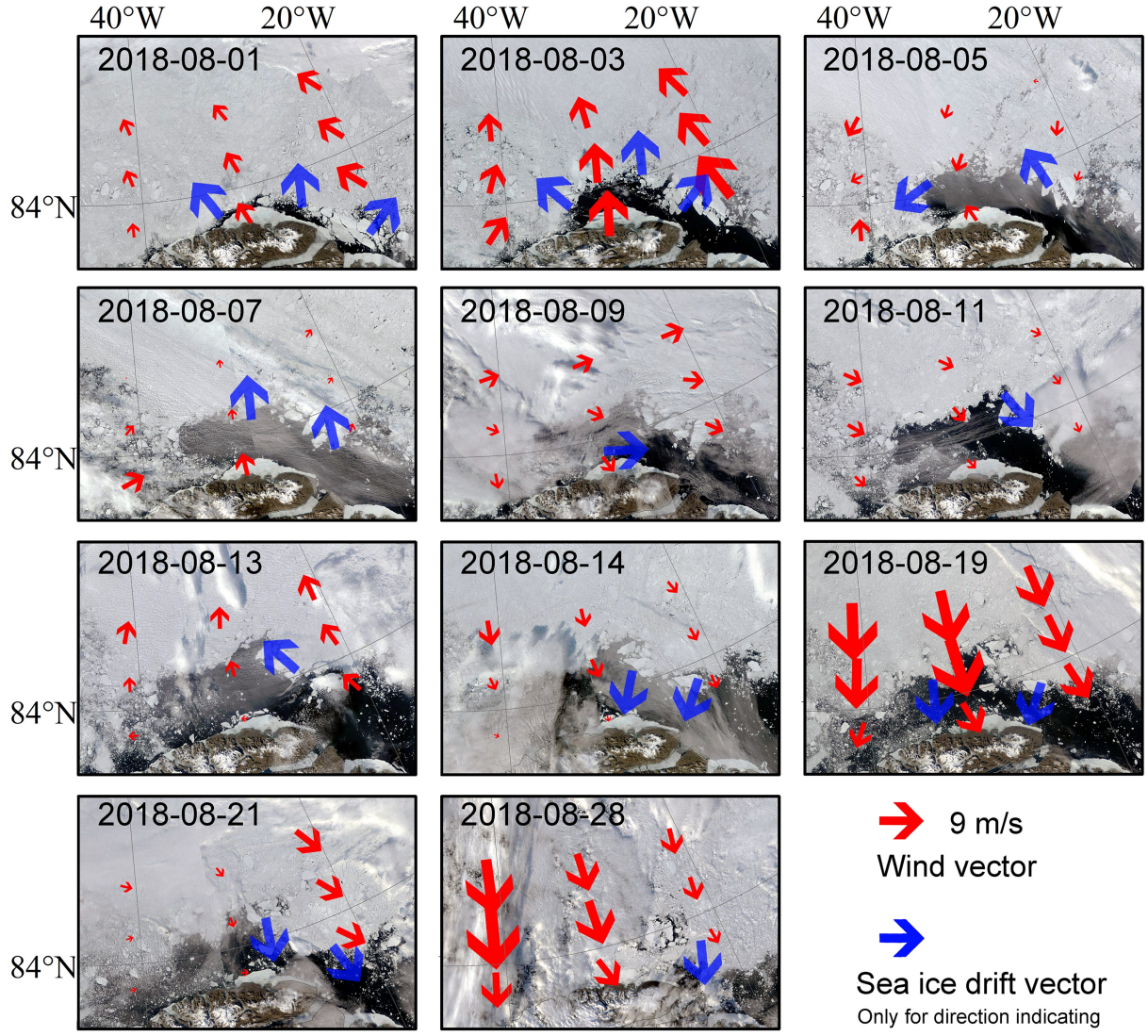

Fig. 6. Time-series of MODIS true-color combination images and wind vectors in August 2018. The blue arrows indicate sea ice drift vectors and red arrows represent wind vectors. The wind vectors were derived from ERA5 data. The sea ice drift vectors can only be used to indicate direction.

impacts on ice break up would require more accurate in situ long term observations.

3.3. *Comparison to the previous polynyas*

As was mentioned earlier, the main mechanism for previous polynya opening in the Arctic is regional wind, hence the timing, area and duration of a polynya are usually variable (Morales-Maqueda et al., 2004). Arctic polynyas mostly appeared on confined locations near the coast, such as "fast ice edge" and ice shelf. Most previous studies focused on the winter polynyas to quantify the ice production rates and surface energy fluxes. In comparison to these winter polynyas, the August polynya extent is similar (Table 2). Two studies focused on winter polynyas to the north of Greenland: 1) Preußer et al. (2019) found a polynya with an average extent of 2.5×10^3 km^2, and 2) a polynya with a mean length of 5.7 km was found by Winsor and Björk (2000). Much larger polynyas are found in both February and August 2018, which is remarkable in comparison to previous reported polynyas along the north coast of Greenland (Table 2). There are also some polynyas that have appeared in Arctic summer (e.g., Wrangel Island polynya and North-East Water polynya); however, no studies reported the summer polynyas along the north coast of Greenland. Although some winter polynyas have been found to the north of Greenland, remarkable polynyas only occurred in February and August 2018. As these two polynyas appeared in different seasons, atmospheric and ice conditions are different, hence it is helpful to compare the different mechanisms, which will benefit further research and forecasting of polynyas north of Greenland.

The February polynya featured anomalously high T2m, and the wind speed reached an extremely high value (15.3 m s^{-1}) during the polynya period. These results agree with those of previous studies (Moore et al., 2018; Ludwig et al., 2019). Upon comparing to the February event, some cli-

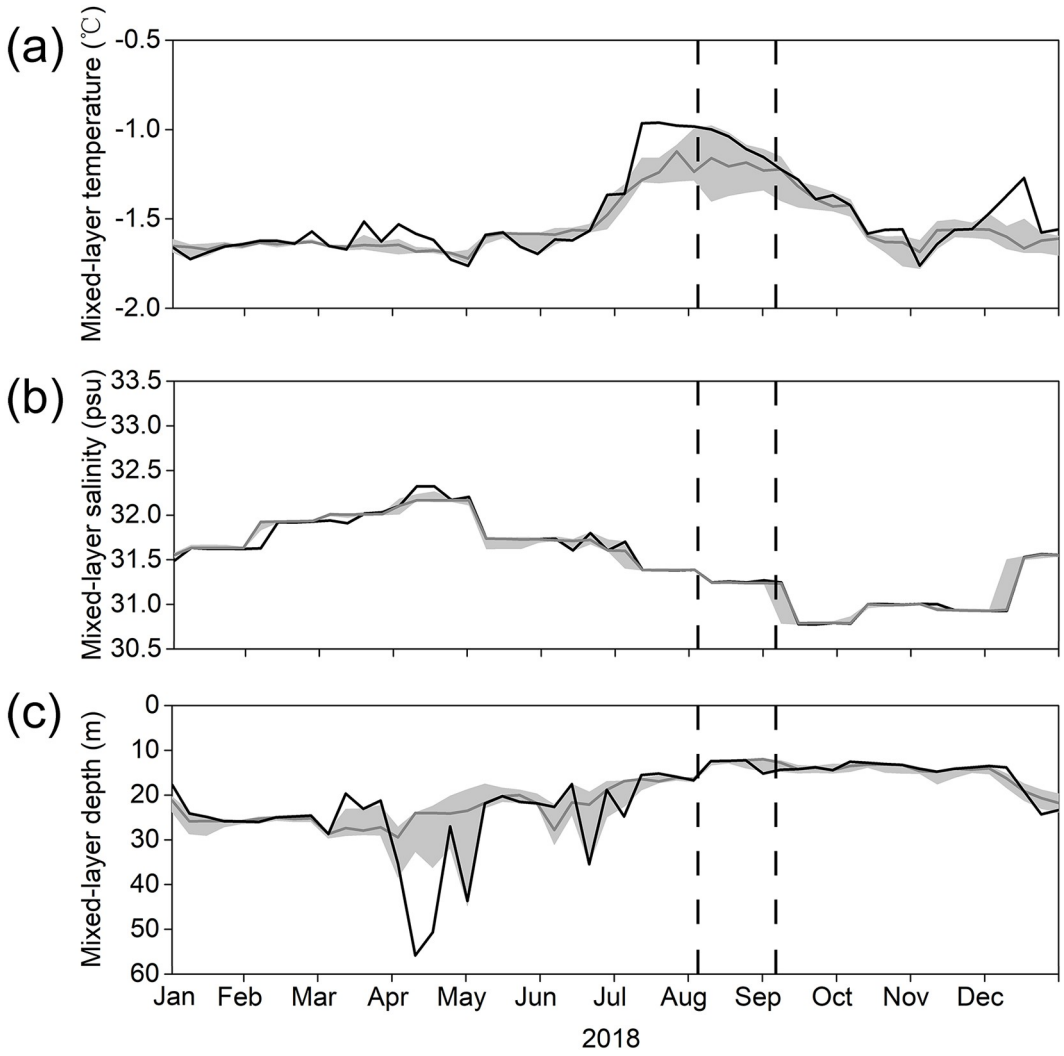

Fig. 7. Mixed-layer properties in the region of interest in 2018. (a) Mixed-layer temperature; (b) Mixed-layer salinity and (c) Mixed-layer depth. Weekly values are shown by black lines. The 2014–18 means are shown by the medians (grey lines) and 25%–75% interquartile ranges are denoted by grey shading. Black dashed lines indicate the polynya period. All these data are taken from E.U. Copernicus Marine Service Information.

mate conditions were found to be different for the August polynya. On the one hand, NAO was positive before the February polynya event, it subsequently decreased during the polynya opening, and then increased during the refreezing. Although the NAO during the August polynya period featured a similar change pattern, all its values were positive. The NAO during the February polynya period was negative since it displayed the maximum extent on 26 February, and this situation was associated with a sudden stratospheric warming (Moore et al., 2018). On the other hand, lower average wind speed was found during the August polynya (3.8 m s^{-1} comparing to 6.1 m s^{-1}, Fig. 5b). We have found that thinner sea ice increases its wind-driven drift (Table 1) and the wind did not have to be as strong as the storm conditions in February 2018 to induce the polynya. Hence, more polynyas are expected to occur in the future as the overall Arctic SIT is continuously decreasing (Kwok, 2018). In terms of the ocean, during the February polynya period, a stable ocean stratification within the climatological boundary was found (Fig. 7). This is similar to that during the August polynya period, as no evidence for the occurrence of upward heat flux was found.

In addition, the peak temperature during the event in February rose almost to the freezing point. The temperatures before and after the event, however, were significantly lower. The temperatures in August polynya were much warmer than those in February polynya (–0.6°C comparing to –16.4°C, from ERA5 data, Fig. 2b). The August polynya occurred before the period of minimum sea ice extent when T2ms were partly above the freezing point, which means that temperatures prevented refreezing in August, while in February they only decreased refreezing. Usually, a narrow lead developed off the ice zone on the north coast of Greenland in summer, and seldom evolved into a polynya like the one that occurred in August 2018. This polynya appeared when SIT was low and thus its formation and closing may also be associated with the seasonal cycle, which is quite different from that in February 2018 when a polynya formed in

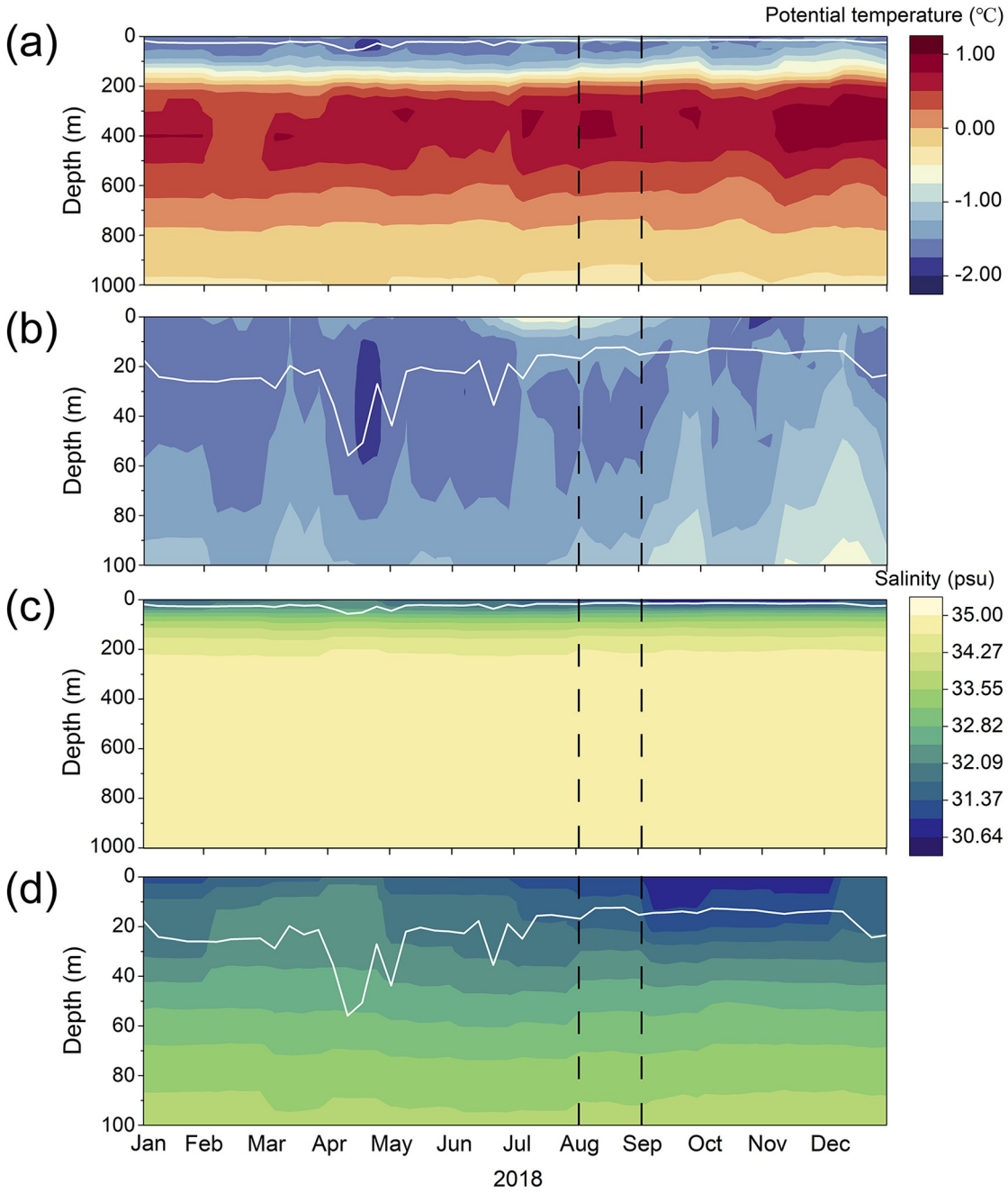

Fig. 8. Ocean property profiling in the region of interest in 2018. (a) potential temperature; (c) salinity. (b) and (d) provide vertically enlarged plots showing the ocean property profiling from the ocean surface to a depth of 100 m for (a) and (c), respectively. Mixed-layer depth values are shown by white lines. All these data are taken from E.U. Copernicus Marine Service Information.

winter with higher SIT. Thinner sea ice in August increased its wind-driven drift and hence modest wind (compared to the anomalously strong wind in February) caused the August polynya opening, hence it was responsible for the formation of the August polynya.

4. Conclusion

In the present study, we conclude that two factors were mainly responsible for the August polynya development. First, the thinnest August sea ice cover since 1979 occurred in 2018, which was due to the continued decreases in SIT in the Arctic. Sea ice drift has become more responsive to the regional wind favoring polynya formation when sea ice cover is becoming thinner. It was found that most of the MYI was replaced by FYI due to the February polynya, a situation that persisted throughout the winter. Hence, the unusual conditions during the winter of 2018 may also have

Table 2. Statistics of the Arctic polynyas in previous studies. Polynya time, study area and extent/length are included.

	Time	Study area	Average extent/ Length
Preußer et al. (2019)	winter seasons from 2002/2003 to 2017/2018	17 Arctic polynya regions (including north of Greenland)	12.4×10^3 km^2
Iwamoto et al. (2014)	winter seasons from 2002/2003 to 2010/2011	10 major Arctic coastal polynyas	58.3×10^3 km^2
Willmes et al. (2011)	winter seasons from 1979/1980 to 2007/2008	Laptev Sea	0.8×10^3 km^2
Martin et al. (2004)	winter seasons from 1990 to 2001	Chukchi Sea Alaskan coast	22.9 km
Winsor and Björk (2000)	winter seasons from 1958 to 1997	28 Arctic polynya regions (including north of Greenland)	6.6 km
Moore et al. (2018)	February 2018	North of Greenland	23.7×10^3 km^2
Moore and Pickart (2012)	summer seasons from 1979 to 2011	Wrangel Island polynya	4.7×10^3 km^2
Gudmandsen et al. (1995)	summer seasons from 1992 and 1993	North-East Water polynya	21.3×10^3 km^2
This study	August 2018	North of Greenland	14.5×10^3 km^2

played an important role as the FYI is easier to move. Second, moderate wind persisted through the polynya period accompanied by the positive NAO. The modest wind speed during August polynya was sufficient to cause sea ice divergence under the thinnest sea ice conditions since 1979, and the sea ice drift pattern was consistent with the regional wind field (southerly), thus wind had a direct effect on the August polynya formation.

This study indicates that the August polynya was caused by the combination of these two factors. Furthermore, our analysis suggests that more polynyas will presumably occur in the Arctic as continuing thinning of sea ice is easier to be moved by wind. This will further influence the atmospheric-ocean heat exchange and the large-scale ice mass balance.

Exact understanding and prediction of Arctic polynya formation requires improved knowledge of both the dynamic (e.g., wind-induced sea ice drift) and thermodynamic (e.g., upwelling heat) processes during the polynya evolution. Unfortunately, the detailed processes are not well known because of limitations imposed by the applied satellite or model data. Sea ice production was not assessed in the present study. Its effects on the fate (e.g. time of opening and extent) of the polynyas in the future are largely unknown. More in situ and satellite data are needed to investigate in detail August polynyas in future studies.

Acknowledgements. This work was supported by the National Key Research and Development Program of China (Grant No. 2018YFC1407206), Academy of Finland (Grant No. 317999), and European Union's Horizon 2020 research and innovation programme (Grant No. 727890-INTAROS).

Data availability

SIC and sea ice drift data were derived from NSIDC at https://doi.org/10.5067/8GQ8LZQVL0VL and at https://doi.org/10.5067/INAWUWO7QH7B, respectively (last accessed date: 20 July 2020); PIOMAS SIT data were obtained at http://psc.apl.washington.edu/zhang/IDAO/data_piomas.html (last accessed date: 20 July 2020); ocean temperature and salinity profiling data were acquired using E.U. Copernicus Marine Service Information at http://marine.copernicus.eu/services-portfolio/access-to-products/?option=com_csw&view=details&product_id=MULTIOBS_GLO_PHY_NRT_015_001 (last accessed date: 20 July 2020); ERA5 reanalysis data were obtained at https://cds.climate.copernicus.eu/cdsapp#!/dataset/reanalysis-era5-single-levels?tab=overview (last accessed date: 20 July 2020); NAO index data were derived from NOAA at http://www.cpc.ncep.noaa.gov (last accessed date: 20 July 2020); meteorological data from the Kap Morris Jesup weather station can be downloaded at https://www.timeanddate.com/weather (last accessed date: 20 July 2020). MODIS image was obtained from NASA worldview application at https://worldview.earthdata.nasa.gov (last accessed date: 20 July 2020).

REFERENCES

April, A., B. Montpetit, and D. Langlois, 2019: Linking the open water area of the north open water polynya to climatic parameters using a multiple linear regression prediction model. *Atmos. Ocean*, **57**(2), 91–100, https://doi.org/10.1080/07055900.2019.1598332.

Campbell, E. C., E. A. Wilson, G. W. K. Moore, S. C. Riser, C. E. Brayton, M. R. Mazloff, and L. D. Talley, 2019: Antarctic offshore polynyas linked to Southern Hemisphere climate anomalies. *Nature*, **570**, 319–325, https://doi.org/10.

1038/s41586-019-1294-0.

Cavalieri, D. J., C. L. Parkinson, P. Gloersen, and H. J. Zwally, 1997: Arctic and Antarctic Sea Ice Concentrations from Multichannel Passive-microwave Satellite Data Sets: October 1978 to December 1996, User's Guide. NASA Technical Memorandum 104647. [Available from: https://nsidc.org/sites/nsidc.org/files/technical-references/NASA%20Technical%20Memorandum%20104647.pdf]

Gudmandsen, P., B. B. Thomsen, L. T. Pedersen, H. Skriver, and P. J. Minnett, 1995: North-East Water polynya: Satellite observations summer 1992 and 1993. *Int. J. Remote Sens.*, **16**, 3307–3324, https://doi.org/10.1080/01431169508954632.

Guinehut, S., A. L. Dhomps, G. Larnicol, and P. Y. Le Traon, 2012: High resolution 3D temperature and salinity fields derived from in situ and satellite observations. *Ocean Sci.*, **8**, 845–857, https://doi.org/10.5194/os-8-845-2012.

Iwamoto, K., K. I. Ohshima, and T. Tamura, 2014: Improved mapping of sea ice production in the Arctic Ocean using AMSR-E thin ice thickness algorithm. *J. Geophys. Res. Oceans*, **119**, 3574–3594, https://doi.org/10.1002/2013JC009749.

Kohout, A. L., M. J. M. Williams, S. M. Dean, and M. H. Meylan, 2014: Storm-induced sea ice breakup and the implications for ice extent. *Nature*, **509**(7502), 604–607, https://doi.org/10.1038/nature13262.

Kwok, R., 2018: Arctic sea ice thickness, volume, and multiyear ice coverage: Losses and coupled variability (1958–2018). *Environ. Res. Lett.*, **13**, 105005, https://doi.org/10.1088/1748-9326/aae3ec.

Kwok, R., G. Spreen, and S. Pang, 2013: Arctic sea ice circulation and drift speed: Decadal trends and ocean currents. *J. Geophys. Res. Oceans*, **118**, 2408–2425, https://doi.org/10.1002/jgrc.20191.

Ludwig, V., G. Spreen, C. Haas, L. Istomina, F. Kauker, and D. Murashkin, 2019: The 2018 North Greenland polynya observed by a newly introduced merged optical and passive microwave sea-ice concentration dataset. *Cryosphere*, **13**, 2051–2073, https://doi.org/10.5194/tc-13-2051-2019.

Martin, S., R. Drucker, R. Kwok, and B. Holt, 2004: Estimation of the thin ice thickness and heat flux for the Chukchi Sea Alaskan coast polynya from Special Sensor Microwave/Imager data, 1990–2001. *J. Geophy. Res. Oceans*, **109**, C10012, https://doi.org/10.1029/2004JC002428.

Minnett, P. J., and E. L. Key, 2007: Meteorology and atmosphere-surface coupling in and around polynyas. *Elsevier Oceanography Series, Elsevier*, **74**, 127–161, https://doi.org/10.1016/S0422-9894(06)74004-1.

Moore, G. W. K., and R. S. Pickart, 2012: The Wrangel Island Polynya in early summer: Trends and relationships to other polynyas and the Beaufort Sea High. *Geophys. Res. Lett.*, **39**, L05503, https://doi.org/10.1029/2011GL050691.

Moore, G. W. K., A. Schweiger, J. Zhang, and M. Steele, 2018: What Caused the Remarkable February 2018 North Greenland Polynya? *Geophys. Res. Lett.*, **45**, 13 342–13 350, https://doi.org/10.1029/2018GL080902.

Morales-Maqueda, M. A., A. J. Willmott, and N. R. T. Biggs, 2004: Polynya dynamics: A review of observations and modeling. *Rev. Geophys.*, **42**, RG1004, https://doi.org/10.1029/2002rg000116.

Mulet, S., M. H. Rio, A. Mignot, S. Guinehut, and R. Morrow, 2012: A new estimate of the global 3D geostrophic ocean circulation based on satellite data and in-situ measurements. *Deep Sea Res. Part II: Top. Stud. Oceanogr.*, **77–80**, 70–81, https://doi.org/10.1016/j.dsr2.2012.04.012.

Parkinson, C., and Coauthors, 1996: Sea ice concentrations from Nimbus-7 SMMR and DMSP SSM/I-SSMIS passive microwave data, Version 1. *NASA National Snow and Ice Data Center Distributed Active Archive Center*, https://doi.org/10.5067/8GQ8LZQVL0VL.

Preußer, A., G. Heinemann, S. Willmes, and S. Paul, 2016: Circumpolar polynya regions and ice production in the Arctic: results from MODIS thermal infrared imagery from 2002/2003 to 2014/2015 with a regional focus on the Laptev Sea. *Cryosphere*, **10**, 3021–3042, https://doi.org/10.5194/tc-10-3021-2016.

Preußer, A., K. I. Ohshima, K. Iwamoto, S. Willmes, and G. Heinemann, 2019: Retrieval of wintertime sea ice production in Arctic polynyas using thermal infrared and passive microwave remote sensing data. *J. Geophys. Res. Oceans*, **124**, 5503–5528, https://doi.org/10.1029/2019JC014976.

Smith, S. D., R. D. Muench, and C. H. Pease, 1990: Polynyas and leads: An overview of physical processes and environment. *J. Geophys. Res. Oceans*, **95**, 9461–9479, https://doi.org/10.1029/jc095ic06p09461.

Squire, V. A., and S. C. Moore, 1980: Direct measurement of the attenuation of ocean waves by pack ice. *Nature*, **283**, 365–368, https://doi.org/10.1038/283365a0.

Sumata, H., T. Lavergne, F. Girard-Ardhuin, N. Kimura, M. A. Tschudi, F. Kauker, M. Karcher, and R. Gerdes, 2014: An intercomparison of Arctic ice drift products to deduce uncertainty estimates. *J. Geophys. Res. Oceans*, **119**, 4887–4921, https://doi.org/10.1002/2013JC009724.

Tschudi, M., W. N. Meier, J. S. Stewart, C. Fowler, and J. Maslanik, 2019: Polar Pathfinder Daily 25 km EASE-Grid Sea Ice Motion Vectors, Version 4. *NASA National Snow and Ice Data Center Distributed Active Archive Center*, https://doi.org/10.5067/INAWUWO7QH7B.

Willmes, S., S. Adams, D. Schröder, and G. Heinemann, 2011: Spatio-temporal variability of polynya dynamics and ice production in the Laptev Sea between the winters of 1979/80 and 2007/08. *Polar Res.*, **30**, 5971, https://doi.org/10.3402/polar.v30i0.5971.

Winsor, P., and G. Björk, 2000: Polynya activity in the Arctic Ocean from 1958 to 1997. *J. Geophys. Res. Oceans*, **105**, 8789–8803, https://doi.org/10.1029/1999JC900305.

Zhang, J. L., and D. A. Rothrock, 2003: Modeling global sea ice with a thickness and enthalpy distribution model in generalized curvilinear coordinates. *Mon. Wea. Rev.*, **131**, 845–861, https://doi.org/10.1175/1520-0493(2003)131<0845:MGSIWA>2.0.CO;2.